Timescale settling and nature of electron transport in magnetite – General considerations in view of new magnetic after-effect results on dilutely Ti^{4+}-doped Fe_3O_4

2005 J. Phys.: Condens. Matter 17 6763

(http://iopscience.iop.org/0953-8984/17/42/014)

INSTITUTE OF PHYSICS PUBLISHING JOURNAL OF PHYSICS: CONDENSED MATTER

J. Phys.: Condens. Matter **17** (2005) 6763–6781 doi:10.1088/0953-8984/17/42/014

Timescale settling and nature of electron transport in magnetite – General considerations in view of new magnetic after-effect results on dilutely Ti^{4+}-doped Fe_3O_4

F Walz[1], **V A M Brabers**[2], **J H V J Brabers**[3] **and H Kronmüller**[1]

[1] Max-Planck-Institut für Metallforschung, Stuttgart, Germany
[2] Department of Physics, Eindhoven University of Technology, Eindhoven, The Netherlands
[3] Philips Centre for Industrial Technology, Eindhoven, The Netherlands

Received 22 July 2005, in final form 12 September 2005
Published 7 October 2005
Online at stacks.iop.org/JPhysCM/17/6763

Abstract

The effect of dilute titanium (Ti^{4+})-doping on the magnetic after-effect (MAE) spectra of stoichiometric magnetite single crystals, $Fe_{3-x}Ti_xO_4$ – with $0.0001 \leqslant x \leqslant 0.008$ – is studied in the temperature range $4\ \mathrm{K} < T \leqslant T_V \simeq 125\ \mathrm{K}$ and analysed in terms of our revised relaxation model. The effects of these relatively low doping rates comprise: (i) strong impact on low-temperature ($4\ \mathrm{K} < T < 35\ \mathrm{K}$) incoherent electron ($e^-$)-tunnelling and combined intra-ionic thermal excitation; (ii) minor, though highly instructive, modifications of thermally activated electron hopping ($50\ \mathrm{K} < T < 125\ \mathrm{K}$), and (iii) low-temperature shifting of the Verwey transition (T_V) relative to the temperature of zero-crossing of the crystal anisotropy (T_{K_1}). Due to the high oxygen stoichiometry of the crystals (absence of B-site vacancies), no further MAEs appear in the high-temperature range ($T > T_V$).

The recently accentuated discussion concerning the appropriate timescale of electron transport – deduced from modern x-ray resonant scattering to be about $\tau \simeq 10^{-16}$ s, over the whole temperature range ($T \gtrless T_V$), in contrast to up to thousands of seconds as determined from high-precision MAE experiments, in the low-temperature phase ($T < T_V$) – gives us the chance to sharpen our arguments in favour of a clarification of the electronic conductivity mechanisms in magnetite.

1. Introduction

Our present paper follows a dual purpose:

(i) to provide an immediate extension of our previous magnetic after-effect (MAE) studies on highly Ti-doped ($0.1 \leqslant x \leqslant 1.0$), non-oxygen-stoichiometric ($\Delta \simeq 0.005$) single-crystalline magnetite, $Fe_{3-x-\Delta}Ti_xO_4$ [1], down to lower Ti contents, varying between $0.0001 \leqslant x \leqslant 0.008$ – in the absence of cation vacancies ($\Delta \simeq 0$) – and

(ii) to draw attention, in view of these recent results, on the extreme sensibility of the electronic processes in Fe_3O_4 – as resolved by means of the MAE – to even smallest lattice perturbations of any kind, like i.e. impurities, non-stoichiometry, point defects, and stresses [1, 2]. As outlined in a recent review, such defect-induced interactions with the electronic system can be most sensitively detected and identified by means of MAE spectroscopy (cf section 2.2) which, consequently, represents a most appropriate tool for quality control and defect analysis of Fe_3O_4 [2].

These latter aspects (ii) are of fundamental importance with regard to the paradoxical situation – known as the 'magnetite dilemma' – that, in spite of many efforts, over a period of about 60 years it has proved impossible to either definitely substantiate or falsify Verwey's initially proposed magnetite model [3] – which, in combination with Mott's theoretical interpretations [4], will be denoted as the Verwey–Mott model henceforth. This model proposes an interconnection between the spontaneous crystallographic transition from lower to cubic symmetry, at $T_V \simeq 125$ K, and the spontaneous breakdown of a low-temperature ionic order state, thereby inducing an increment of the electric conductivity by a factor of about 100. Below T_V, conductivity and MAEs are assumed to result from thermally activated transport of ionically localized electrons.

In view of the still open question concerning the adequacy of Verwey's basic conceptions, two strategies are feasible in order to overcome the existing dilemma.

(1) To undertake enhanced attempts in order to definitely prove or falsify the basic predictions of Verwey's model, i.e., by repeating the decisive experiments on crystals of ultimate quality by techniques of unequivocal significance. This attempt appears necessary, however, since insufficient quality of investigated magnetite crystals has been identified as a source of frequent misinterpretations in the past – and still in the present [2]. For instance, quality deficiencies characterized by a reduction of the Verwey temperature – i.e., the most simple crystal quality parameter – of about only $\leqslant 3$ K from the ideal value (of $T_V \simeq 125$ K) already have detrimental consequences on the MAE spectra – and hence on the associated electronic transport processes – as clearly demonstrated in our present experiments, cf figures 1–3 with figure 4. Thus, crystal quality of highest perfection must be a condition of *sine qua non* if respective results are made a basis for far-reaching model revisions [5, 6].

Even worse, the tendency of inattentive generalization of results obtained on imperfect magnetite – due to deficiencies of various nature like, for example, crystallography, stoichiometry, lattice defects of any type, including geometric constraints – is even increasing due to the modern demand on Fe_3O_4-based magneto-electronic sensors of reduced geometrical dimensions like films, sheets, multilayers, powders, etc [7–11]. Similar care has to be taken in the use of rather surface-limited techniques – even when applied on perfect bulk crystals – such as x-ray resonant scattering (XRS) [5, 6], the magneto-optical Kerr-effect [8], scanning tunnelling microscopy [12], photoemission spectroscopy [13], and x-ray magnetic circular dichroism (XMCD) [14].

(2) An alternative, rather impetuous strategy tries to settle the open magnetite dilemma by regarding the Verwey model – due to its lacking experimental verifiability, despite so many decade-long (though frequently inappropriate) efforts – already by now as being definitely discarded. This attitude has been accentuated recently in view of modern XRS experiments which did not reveal any variation of respective spectra over the whole temperature range $4\ \text{K} < T < 350$ K and – most surprisingly – not even upon crossing the Verwey transition [5, 6]. This observation, regarded by the authors as ultimate proof against the Verwey model, has been interpreted in terms of lacking charge difference

between the octahedrally (B) sited Fe ions. Assuming therefore all B-sited Fe ions to be electronically – and hence also magnetically – equivalent, atomic electron localization below T_V is completely ruled out, as well as any type of ionic ordering within the whole temperature range $T \gtrless T_V$. Accordingly, all electrons are assumed to occupy itinerant band-states, characterized by fluctuations of the order of 10^{-16} s – corresponding to the electron–x-ray interaction times.

From a realistic point of view, one recognizes immediately that conception (2) – since it completely ignores well-established results acquired by means of highly sensitive MAE and electronic conductivity (EC) techniques – cannot comprise the full truth. Thus, the mere occurrence of pronounced MAEs below T_V is incontestable evidence of the existence of, at least, two magnetically – and hence also electronically – different types of Fe ions residing on octahedral sites – in contrast to type (2) arguing. Between these unequal ions thermally activated electron exchange takes place, giving rise to magnetic relaxation processes (MAEs) – in addition to inherently related conductivity mechanisms – within timescales amounting up to thousands of seconds [2]. Reconciliation between these diverging type (1) and type (2) interpretations appears feasible – putting aside here possible objections against sample quality ($T_V \lesssim 121$ K) and x-ray penetration depth of category (2) experiments – by stating type (1) and type (2) techniques to be sensitive on differently conditioned electrons, i.e. type (2)-sensitive electrons residing on filled bands (groundstate), being characterized by fluctuation times of the order of x-ray–electron interaction (10^{-16} s) in contrast to type (1)-sensitive electrons, residing in the excited state, undergoing thermally activated local exchange between adjacent, magnetically different B-sited Fe ions, thereby inducing MAEs within extended timescales (up to $\gtrsim 10^3$ s). Under these aspects, the alternative experiments are unable to provide equally detailed information on the specific electronic processes taking place in the different states but, instead, are either confined on (1) the technologically most interesting magnetic relaxation and electric conductivity mechanisms in the excited state or (2) rather related with electronic phenomena being typical for the filled band groundstate.

The high sensitivity of the MAE on thermally activated magneto-electronic relaxation processes in magnetite is based on two elementary, system-immanent peculiarities: (a) the time-dependent magnetocrystalline interaction of the spontaneous domain wall magnetization with a huge number of identical, *anisotropic* lattice defects residing within the *macroscopic* sphere of influence of the domain wall – thereby inducing an eminent amplification of the individually, locally arising atomic interactions – and (b) the inherent coupling of local charge and anisotropy transport between neighbouring, B-sited Fe ions of different valencies, as symbolically expressed by the formulae

$$\text{“Fe}^{3+}\text{”} + e^- \rightleftarrows \text{“Fe}^{2+}\text{”}, \qquad \text{or} \tag{1a}$$

$$\text{“Fe}_1^{3+}\text{”} + \text{“Fe}_2^{2+}\text{”} \rightleftarrows \text{“Fe}_1^{2+}\text{”} + \text{“Fe}_2^{3+}\text{”}. \tag{1b}$$

The apostrophized symbols in equation (1) indicate that – deviating from the original Verwey–Mott model – we are conceding in the following the occurrence of non-integral, though definitely non-equivalent, ionic valencies as discussed in recent electron-theoretical essays, (section 4.2.1)[4]. It is especially this intimacy between charge (electron) and local anisotropy

[4] As the driving force for the combined electron – anisotropy transport according to equation (1), we regard the different orbital magnetism of Fe^{2+} and Fe^{3+} ions, resulting – as an *artefact* – from the originally different free Fe ion groundstates which are assumed to further differ, residually, despite crystal field quenching, even in the inverse spinel lattice. Thus, in the case of Fe^{3+}, 5d-electrons (d^5) yield, according to Hund's rules, zero-orbital momentum and hence magnetic isotropy, as denoted by $^6S_{5/2}$, whereas Fe^{2+}, due to its 6d-electrons (d^6), possesses a groundstate orbital momentum – and hence magnetic anisotropy – as denoted by ($^5D_4$), [15, 16]. Against this background, the various MAE processes occurring in magnetite have as common source the orientation of such *local*

transport – the latter giving rise to pronounced magnetic relaxations – which constitutes the unique sensitivity of the MAE technique on the low-temperature electron-based conductivity mechanisms, of type (1), in magnetite and related ferrites.

Interestingly, local valency–anisotropy exchange in magnetite, according to equation (1), is feasible by two different mechanisms based on either (i) *electronically* or (ii) *ionically* supported charge transfer – as confirmed experimentally in the form of two well-distinguished types of MAE spectra [1, 2, 18–22] residing, respectively, below and above T_V. The conditions supporting these two types of charge-anisotropy transfer, however, are completely opposite: *ionically induced relaxations* – confined to the high-temperature range ($T > 125$ K), preferentially around 300 K – owe their existence to the presence of *lattice defects*, i.e. cation vacancies and/or impurity atoms [17, 20–22] and, consequently, are *completely absent* in perfect crystals; on the other hand, *electronically induced relaxations* – associated, for example, with incoherent electron tunnelling ($4\ \text{K} < T < 35$ K) and thermally activated electron hopping ($50\ \text{K} < T < 125$ K), [2, 15–20] – are fully developed only in *stoichiometric, completely defect-free* magnetite, becoming severely affected – and frequently completely suppressed – in the presence of even smallest lattice perturbations.

Our present and previous [1] series of experiments on $Fe_{3-x-\Delta}Ti_xO_4$ are, respectively, instructive examples of these two, electronically and ionically induced, types of relaxation mechanisms in magnetite-based ferrites. In particular, the present investigations, on stoichiometric, Ti(x)-doped magnetite ($\Delta = 0$; $0.0001 \leqslant x \leqslant 0.008$), offer novel insights into the interdependences between low impurity doping and the intrinsic, electronically supported conductivity mechanisms, thereby providing relevant arguments concerning the fundamental questions in the still remaining magnetite dilemma.

2. Experimental techniques

2.1. Specimens

The $Fe_{3-x}Ti_xO_4$ single crystals studied in our experiments were prepared from Fe_2O_3 and TiO_2 by means of a floating zone technique [1, 23]. After crystallization – in the form of rods with their axis oriented along ⟨110⟩ and typical dimensions of 30 mm length and 5 mm diameter – the samples were carefully annealed for 70 h at 1403 K in an appropriate CO_2–H_2 atmosphere which, upon subsequently cooling down to room-temperature, was continuously adjusted so as to always keep the Fe_3O_4 phase equilibrium [24, 25] and thus to avoid any deviations from stoichiometry, being incited, for example, by the introduction of octahedral vacancies [2, 17, 21]. In preparation for the MAE measurements, these rods were cut by spark erosion into prisms with dimensions of 20 mm × 1.4 mm × 1.4 mm.

The stoichiometric reference single crystal (figure 1), grown with the same crystallographic symmetry by using principally the same technique (starting from α-Fe_2O_3 [26]), was measured in its as-produced cylinder geometry of about 30 mm length and 8 mm diameter.

2.2. Measuring technique

The *isochronal* MAE spectra discussed in the following are constructed by systematically arranging, along the temperature axis (cf figures 1–3), the accumulated amount of *isothermal*

"Fe^{2+}"-type anisotropies – due to thermal activation of either electron exchange (incoherent tunnelling or hopping, as intrinsic processes in perfect magnetite) or ionic migration (e.g., vacancy-mediated hopping of "Fe^{2+}"-ions, in nonstoichiometric crystals) – in relation to the spontaneous domain wall magnetization, thereby causing a lowering of the anisotropy interaction potential and hence a reduction of the domain wall mobility, giving rise to the macroscopically observable MAEs [1, 2, 15–22].

relaxation data of the *initial reluctivity* $r(t, T)$-defined, i.e., as the *reciprocal initial susceptibility*: $r(t, T) = 1/\chi(t, T)$ – thereby interconnecting all data points which have been measured at the same time. The various, individual isotherms are obtained by incrementing the measuring temperature in relatively small steps, of ($\Delta T \gtrsim 1$ K), over a wide range of typically 4 K $< T <$ 500 K – thereby using an extremely sensitive, automated LC-oscillator technique, with a measuring frequency of about 1 kHz [27]. Out of these isotherms – whose observation is usually started at $t_1 = 1$ s after sample demagnetization and continued over a standard interval of 2 s $\leqslant t_2 \leqslant$ 180 s – respective isochronals are obtained in the following way:

$$\frac{\Delta r}{r_1} = \frac{\Delta r(t_1, t_2, T)}{r(t_1, T)} = \frac{r(t_2, T) - r(t_1, T)}{r(t_1, T)}. \tag{2}$$

This type of data presentation has the inherent advantage of immediately separating multiprocess relaxations into their different constituents, all of which contributing individually – i.e., in the form of peaks, plateaus, etc – to the observed overall MAE spectrum [1, 2, 15–22, 27–30].

3. Experimental results

3.1. Perfectly stoichiometric magnetite

As basic reference for comparing the drastic influence of even faint Ti-doping on the inherent MAE spectra of Fe_3O_4, we regard the pronounced MAE spectrum of figure 1, being characteristic for magnetite single crystals of highest quality with respect to crystallography, purity and stoichiometry [2]. This standard spectrum has been carefully numerically analysed, using mathematical techniques – i.e. approximations in terms of single (30 K peak) or continuously superimposed Debye-processes (plateaus extending between 4 K $< T <$ 25 K and 50 K $< T <$ 125 K) – which, *a priori*, are independent of any specific underlying model conceptions [2, 17, 18], cf table 1. Only in the case of successful numerical approach

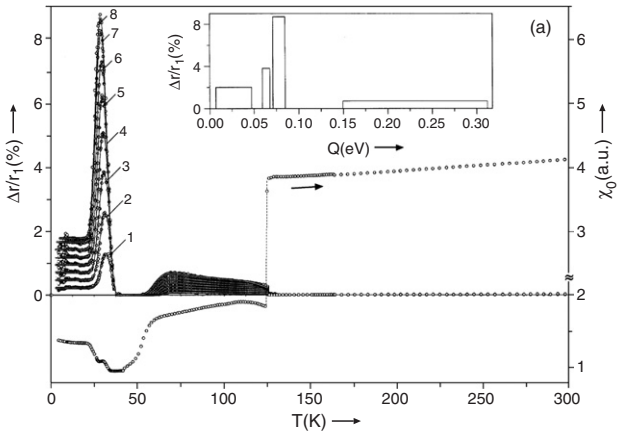

Figure 1. Standard MAE spectrum of perfectly stoichiometric, single-crystalline Fe_3O_4, together with initial susceptibility, χ_0, indicating the Verwey transition by a spontaneous increment near 125 K. Various isochronals of the spectrum are marked by the times t_1 and t_2, elapsed after sample demagnetization (cf section 2.2), i.e., $t_1 = 1$ s; (1) $t_2 = 2$, (2) 4, (3) 8, (4) 16, (5) 32, (6) 64, (7) 128, (8) 180 s. The experimental data (symbols) of the various processes are numerically fitted (continuous lines) and their underlying energy distributions are depicted in the inset.

may the obtained quantitative activation data be helpful in finding appropriate models as a framework for an explanation of the observed spectra. For ease of comparison with the preceding argument [1, 2, 15–22], we keep in the following to our – model-invariant – standard notation for characterizing the various low-temperature MAE processes, i.e. in terms of single (30 K peak) or continuous thermal excitation, the latter being achieved by means of incoherent tunnelling (4 K $< T <$ 25 K) and hopping of electrons (50 K $< T <$ 125 K), respectively.

3.2. Characteristics of the MAE spectra in dilutely Ti-doped magnetite

3.2.1. Low-temperature incoherent electron tunnelling (4 K $< T <$ 35 K). By comparison with the standard spectrum of perfectly stoichiometric magnetite (figure 1) it becomes evident to what extent even weak Ti-doping ($0.0001 \leqslant x \leqslant 0.008$) is able to affect especially the

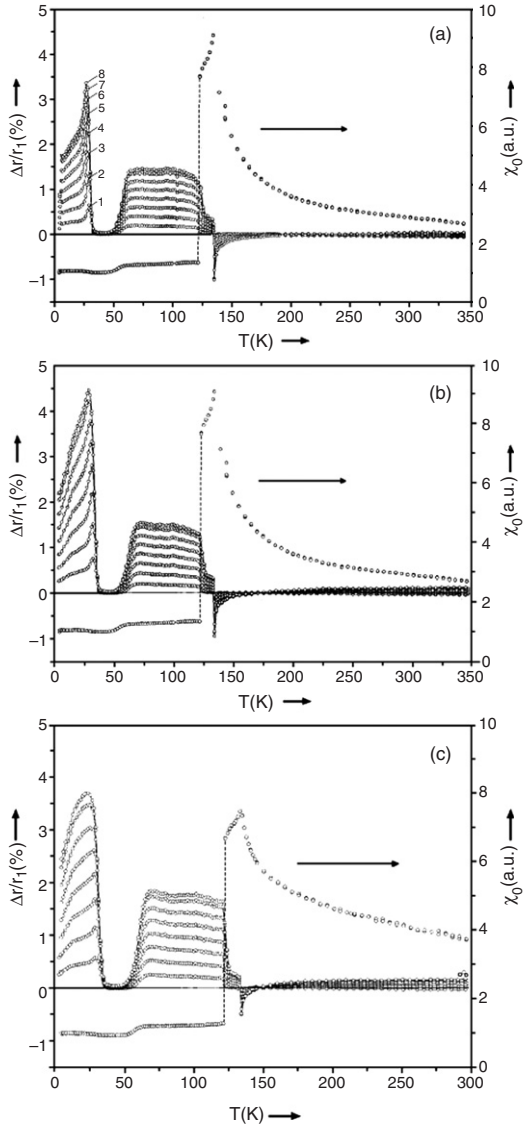

Figure 2. MAE spectra, together with initial susceptibility of single-crystalline $Fe_{3-x}Ti_xO_4$ after doping to the following contents (section 2.1): (a) $x = 0.0001$; (b) $x = 0.0004$ and (c) $x = 0.001$; experimental details as noted in figure 1.

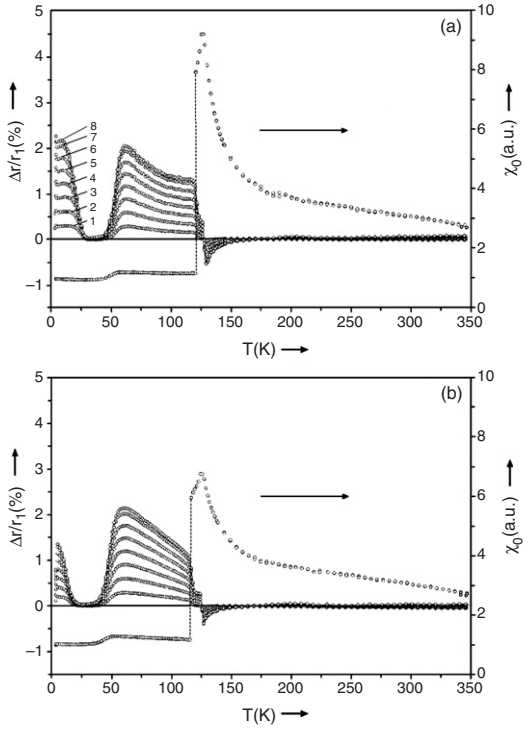

Figure 3. MAE spectra, together with initial susceptibility of single-crystalline $Fe_{3-x}Ti_xO_4$ after doping to the following contents (section 2.1): (a) $x = 0.003$; (b) $x = 0.008$; experimental details as noted in figure 1.

lower-temperature, tunnelling-dominated part of the spectrum (figures 2 and 3; section 1) which, in perfect magnetite, is composed of a characteristic plateau (4 K $< T <$ 25 K) ending in a final Debye peak near 30 K (figure 1). Typically, already for the smallest Ti content (0.0001; figure 2(a)), the tunnel-plateau is considerably deformed, with its upper temperature amplitudes increased up to the top of the Debye peak, thereby indicating an intermixing of these two, normally well-distinguished relaxation modes. This trend is steadily continued upon increased doping ($0.0001 \leqslant x \leqslant 0.001$; figures 2(a)–(c)), ending finally in one single broad relaxation whose upper decay is systematically shifted from 35 K to below 20 K ($x = 0.008$), cf figures 2 and 3. This same high sensibility of low-temperature tunnelling against any type of lattice defects – e.g., ionic substitutions, induced vacancies, internal stresses, etc – has been observed, as a common feature, in numerous preceding investigations, cited in [2, 22].

3.2.2. Thermally activated electron hopping (50 K $< T <$ 125 K). Electron hopping in the temperature range 50 K $< T <$ 125 K (section 1) appearing, at first, less sensitive on Ti-doping over the given range than low-temperature tunnelling ($T <$ 35 K), on closer inspection, however, reveals the plateau amplitude to be increased by about a factor of 3 and its width to become steadily reduced, as indicated by a remarkable low-temperature shifting of the Verwey transition (section 3.2.3). For higher doping rates ($x = 0.003, 0.008$; figure 3), the plateau, moreover, becomes disequilibrated – i.e. in the form of a relative increase of the lower- over the higher-temperature amplitudes – thus indicating an impurity-induced preference for lower-energy hopping.

Table 1. Survey of the various MAE processes occurring in the temperature range 4 K $< T <$ 500 K with typical activation data – T: activation temperature, $Q \pm \Delta Q$: central activation enthalpy and width of enthalpy spectrum, respectively, τ_0 pre-exponential factor (equation (4)) – as thoroughly described in the given references. These processes are traditionally classified from V to I [52], beginning with the – here especially interesting – electronic low-temperature processes (V: 4 K $< T <$ 125 K), followed by relaxations due to intrinsic lattice defects, like interstitials (IV: $\simeq$200 K) and B-site vacancies (III: $\simeq$300 K) to MAEs resulting from interactions between intrinsic (i.e. B-site vacancies) and extrinsic (i.e. substitutional impurities) defects (II: $\simeq$400 K and I: $\simeq$600 K). Process I – being not fully understood, as yet, and hence controversially discussed [52, 53] – lies outside our present considerations and therefore has been omitted from the table.

Process	T (K)	$Q \pm \Delta Q$ (eV)	τ_0 (s)	Mechanisms	References
V_{1A}	$4 < T < 20$	0.03 ± 0.02	$1.0 \times 10^{-10\pm1}$	Incoherent electron tunnelling	[2, 15–22]
V_{1B}	30	0.07 ± 0.01 0.08 ± 0.01	$1.0 \times 10^{-12\pm1}$	Intra-ionic excitation (2-fold superposition)	
V_2	$50 < T < 125$	0.25 ± 0.10	$1.0 \times 10^{-12\pm1}$	Variable range electron hopping	
IV	$\simeq$200	0.70 ± 0.05	$1.0 \times 10^{-14\pm1}$	Intrinsic interstitial reorientation	[1, 2, 18, 22]
III_1 III_2	300	0.85 ± 0.05 0.91 ± 0.05	$7.0 \times 10^{-15\pm1}$	B-site vacancy-mediated Fe^{2+}-hopping	[2, 17–22]
II	$\simeq$400	1.20 ± 0.05	$1.0 \times 10^{-14\pm1}$	Modified 300 K process, due to defect (impurity) interactions	[1, 2, 17–21]

3.2.3. Verwey transition. In addition to the sensitive reactions of the MAE spectra, further information on lattice–defect interactions can be deduced from the temperature dependence of the initial susceptibility, χ_0, cf figures 1–3. Thus, the χ_0-curves of differently Ti-doped samples start, at $T > 4$ K, from a low level extending, without significant temperature dependence, up to about $T \simeq 50$ K. There, they undergo a minute, step-like growth – concomitantly with the onset of the hopping-induced plateau relaxation (50 K $< T < T_V$). With, again, only faint temperature dependence – i.e. increasing on doping between $0.0001 \leqslant x \leqslant 0.001$ and weakly decreasing for $x = 0.003$ and 0.008 – these curves are proceeding up to T_V where, due to the Verwey transition, they undergo a pronounced increment. Typically, near T_V these susceptibility curves assume a cusp-like shape caused by a temperature lag, ΔT_{VC}, between the Verwey transition and the zero-crossing of the crystal anisotropy constant K_1 [31]. This zero-crossing, inducing the sharp susceptibility summit, is followed by a rapid dropping of K_1 to negative values [32] which, in turn, is causing the respective decay of χ_0 on further heating (figures 2–3). Similarly shaped susceptibility curves, as observed previously in other ferrite systems, are thoroughly discussed in [31] with regard to their most prominent representative: $Fe_{3-x}Co_xO_4$.

Moreover, upon closer inspection of these χ_0-curves, a systematic shift of the Verwey temperature is observed from $T_V \simeq 122.5$ to 115.6 K with increasing Ti-doping ($0.0001 \leqslant x \leqslant 0.008$), cf figure 4(a), in addition to a rather temperature-independent gap ΔT_{VC} (figure 4(b))[5] [31].

[5] By comparing the characteristics of the χ_0-curves of stoichiometric (figure 1) and Ti-doped Fe_3O_4 (figures 2–3), it is obvious that both T_V-shifting and the occurrence of a lag ΔT_{VC} between the Verwey transition and zero-crossing of K_1 are impurity induced. The rapid decay of χ_0 on further heating, above K_1 zero-crossing, in the Ti-doped samples – as opposed to the stoichiometric single crystal – however, seems to be rather an effect of sample geometry: i.e., prisms of 1.4 mm × 1.4 mm × 20 mm (Ti-doped crystals) and rod of about 30 mm length and 8 mm diameter

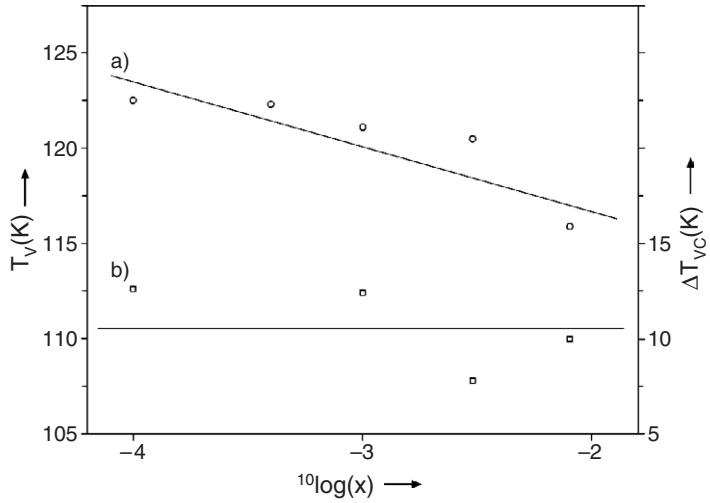

Figure 4. (a) Ti^{4+}-induced shift of the Verwey transition (T_V) to lower temperatures; (b) doping-invariant gap (ΔT_{VC}) between T_V and the temperature of zero-crossing of the anisotropy constant $K_1(T)$.

Comparing the χ_0 curves of the Ti-doped samples (figures 2–3) with that of the stoichiometric crystal (figure 1), we realize that, besides a certain qualitative agreement, the latter one – corresponding to its more pronounced, better-defined MAE spectrum – contains the more detailed information. For instance, the stepwise decrease of χ_0 in the temperature range of the thermally activated Debye process (20 K $< T <$ 35 K, cf figure 1) points clearly to the composed nature of this peak – which has been confirmed, indeed, by means of detailed numerical analysis of the respective MAE data [17, 18], table 1. Typically, for perfect magnetite, both the Verwey transition and zero-crossing of K_1 are coinciding ($\Delta T_{VC} = 0$, cf figure 1), with χ_0 – in contrast to the Ti-doped samples – slowly, but steadily, increasing on further heating in the range $T > T_V$ (see footnote 5).

4. Discussion

4.1. MAE-based timescale settling for electronic charge-transport processes below T_V

Regarding the enormous lag, of about 20 orders of magnitude, between the electronic relaxation times as (1) directly measured in MAE experiments (up to $>10^3$ s) and (2) deduced from x-ray resonant scattering, XRS (10^{-16} s), it is suggestive to conclude that these techniques are susceptible to interactions with different categories of electrons. Thus, the ultra-short fluctuation times associated with type (2) experiments appear compatible with, for example, interactions between x-rays and electrons in completely filled bands, far away from the Fermi level, whereas type (1) experiments are related with electrons which – being situated near the Fermi limit on the borders of a gap, separating two bands – are able to change their energetic states by means of thermal activation.

(single crystal), cf section 2.1. Thus, it appears suggestive to attribute the different shapes of respective χ_0 curves to an additional, geometric, anisotropy contribution becoming active only in the lower-dimensioned samples.

The order of the timescale of corresponding thermally activated relaxations may be quickly reviewed by regarding the case of a single activated Debye process[6], being characterized by the relaxation function, cf [1, 29, 30]:

$$G(t, T) = 1 - \exp(-t/\tau), \tag{3}$$

whose amplitude factor, here normalized to unity, is supposed to remain constant over the relatively narrow temperature range covered by the relaxation maximum. In (3) τ stands for the relaxation time of the process

$$\tau = \tau_0 \exp(Q/kT), \tag{4}$$

with Q the activation enthalpy, k the Boltzmann constant and τ_0 the time-limiting pre-exponential factor – ranging between 10^{-6} s $< \tau_0 <$ 10^{-13} s, depending on type and temperature range of respective processes in various ferrite systems, cf table 1, [2, 17–22]. The condition for extremum (normalized) relaxation strength, $[G(t_2, T) - G(t_1, T)]$, cf equation (3), with respect to T yields a general, temperature-independent relation for the relaxation time at the temperature of the peak maximum [28–30]:

$$\tau(T_{\mathrm{Max}}) = \frac{t_2 - t_1}{\ln(t_2/t_1)}, \tag{6}$$

which, for our experimental conditions ($t_1 = 1$ s, $t_2 = 180$ s, cf section 2.1) assumes a value of about

$$\tau(T_{\mathrm{Max}}) \simeq 35 \text{ s}. \tag{7}$$

It is only by reasons of time-economy when we limit our experimental window to $t_2 = 180$ s – instead of extending it to hours – the chosen *standard frame* (1 s $\leqslant t_2 \leqslant$ 180 s) being wide enough to determine with sufficient accuracy the activation parameters of respective dynamic processes.

The absolute proof for the common origin of magnetic relaxations and corresponding charge transport processes, cf section 1, has been furnished by concomitant measurements of conductivity and MAE on the same stoichiometric Fe_3O_4 single crystal, yielding consistent activation data in both cases [33]. Most interestingly thereby, the thermal activation of electric conductivity is found – within the temperature ranges corresponding to magnetic plateau-type relaxations: 4 K $< T <$ 25 K and 50 K $< T <$ 125 K, cf figures 1 and 5 – to follow the typical '$T^{-1/4}$ relation', as derived by Mott in view of variable range polaron hopping [4, 34]:

$$\sigma(T) = A \exp(-B/T^{1/4}). \tag{8}$$

Even more instructive, in these investigations the pronounced 30 K Debye peak (cf figure 1) is found to have no traceable effect on the observed conductivity behaviour, cf section 4.2.2b.

[6] This estimation of the appropriate timescale remains valid, as well, in the case of narrow superpositions of Debye processes, giving rise to the extended relaxation plateaus discussed in section 3. This becomes evident by recalling that – as described in more detail in [1] – such plateaus may be appropriately approached by assuming their activation enthalpies, Q – or via equation (4), corresponding relaxation times, τ – to follow a rectangular, box-type distribution of constant amplitude over a given interval $\tau(Q_1) < \tau(Q) < \tau(Q_2)$. Under these conditions the following relaxation function holds:

$$G(t, T) = 1 + \frac{1}{\ln \frac{\tau_2}{\tau_1}}\left[\mathrm{Ei}\left(-\frac{t}{\tau_2}\right) - \mathrm{Ei}\left(-\frac{t}{\tau_1}\right)\right], \tag{5}$$

with $\mathrm{Ei}(-1/\tau_i)$ the so-called exponential integral [29, 30].

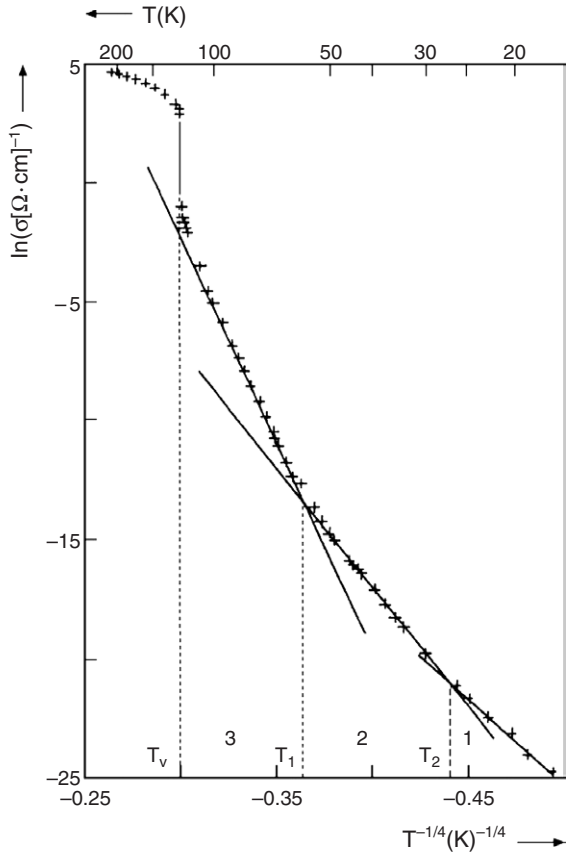

Figure 5. Temperature dependence of the electric conductivity in perfectly stoichiometric, single-crystalline magnetite (same material as in figure 1). Except for the spontaneous jump at T_V, indicating the Verwey transition, thermal activation is observed within the whole temperature range (4 K $< T <$ 350 K). Whereas in the low-temperature intervals 4 K $< T < T_1 \simeq$ 25 K and $T_2 \simeq$ 50 K $< T < T_V \simeq$ 125 K this activation follows the '$T^{-1/4}$-law' (equation (8)), being typical for variable-range particle diffusion (section 4.1), in the temperature range above T_V, a modified, rather linear temperature dependence is observed [33].

4.2. Timescale-conform designing of MAE models

Our considerations so far yielded the clear result that the timescales of those electrons engaged in the technologically most interesting, thermally activated low-temperature processes in magnetite and other ferrites – called thermally excited electrons henceforth – are of the order of seconds up to thousands of seconds. Thus, ultra-short fluctuation times (10^{-16} s), as discussed in connection with modern x-ray diffraction experiments [5, 6], belong, evidently, to itinerant interatomic groundstate transitions which – in contrast to the postulations of [5, 6] – are not able to provide us with any information on thermally excited electrons. Thus, strictly speaking, it is not justified at all to regard the observations made for the ultrashort fluctuations – i.e., lack of low-temperature charge localization and ionic ordering (as basic ingredients of the Verwey–Mott model) – as representative of thermally excited conduction electrons. On the other hand, however, it remains true – not the least due to the reasons discussed in section 1 – that these, Verwey–Mott inherent, features are still lacking definite experimental proof.

Against this background of (i) restricted relevance of XRS observations with respect to MAE and EC results but (ii) lacking experimental proof of the Verwey–Mott conceptions, so far, we try in the following to develop an 'elementary explanation frame' confined only to experimentally indisputable MAE and EC results, being discussed in terms of the most plausible, experimentally supported conceptions available at present.

4.2.1. Necessary precondition for the evolution of MAEs. The driving force for the occurrence of MAEs in Fe_3O_4 and related ferrites consists in the existence of (at least) two magnetically – and hence also electronically – different Fe ions on octahedral spinel sites. Consequently, the indistinguishability of such sites in recent XRS experiments [5, 6] is one of the main arguments for regarding respective results as irrelevant for a better understanding of the technologically important transport mechanisms of conduction electrons in ferrites. On the other hand, the MAE-certified presence of electronically different Fe ions on B-sites is supported by recent high-resolution x-ray and neutron powder diffraction [35] in addition to magneto-optical Kerr effect [36], photoconductivity [13] and XMCD experiments [14]. Interestingly, however, electron-theoretical analysis of these results, on the basis of LSDA + U (local-spin-density-approximation under consideration of Coulomb interactions [37]), yields instead of different, integer-valent Fe ions – i.e., Fe^{2+} and Fe^{3+}, according to Verwey – charge disproportionations of respective ions of the order of $Fe^{2.4+}$ and $Fe^{2.6+}$ [38, 39]. These results, however, notwithstanding the arising complication of charge disproportionation, are in qualitative agreement with the fundamental precondition for the occurrence of MAEs, namely, the existence of electronically *inequivalent* Fe ions on B-sites.

Interestingly, the analysis of these data by means of LSDA + U techniques yields – as supposed also in the Verwey–Mott model – the formation of a gap[7], on cooling below T_V, by splitting of the 3d-t_{2g} states into an occupied lower and an empty higher band [38]. Additionally, these calculations predict charge ordering of conduction electrons, being supported by a concomitant ordering of B-sited Fe^{2+} orbitals [35, 38]. As compared to Verwey's original ordering model, however, the mathematically determined ionic ordering scheme here is of more complicated structure [35], giving rise – due to a collective, order-specific screening of individual ionic charges – to the determined charge disproportionations of +2.4/ + 2.6 (instead of +2.0/+3.0), in addition to a [001]-orientated charge density wave. A further item of this ordering scheme consists in the violation of the Anderson condition [40], as a consequence of taking additionally into account – besides the Coulomb interactions – also elastic potentials arising from the strong lattice distortions[8] induced during the Verwey transition [38, 39].

Though these mathematical models, clearly, cannot replace the direct experimental proof of the fundamental Verwey–Mott conceptions, they, nevertheless, are in qualitative agreement

[7] The Verwey–Mott model explains the appearance of thermally activated processes in the low-temperature magnetite phase as being due to a spontaneous band splitting on cooling below T_V, thus giving rise to the formation of a gap, separating a full valency – from a depopulated, nearly empty conduction band. The latter one is expected to be narrowed to such an extent as to cause ionic electron localization, supporting charge carrier transfer in form of thermally activated polarons [3, 4].

[8] These lattice distortions have a pronounced effect on the low-temperature NMR spectrum [41] which – as expected from a crystallographic symmetry transition at T_V from cubic to monoclinic (C_c) – is split-off, from only two lines (at $T > T_V$), to 24 lines (at $T < T_V$), corresponding to the 8 tetrahedrally (A)- and 16 octahedrally (B)-sited Fe ions in the Fe_3O_4 unit cell. Most interesting in the present context are the observations that (i) on crossing T_V to higher temperatures, due to motional narrowing – i.e., a change of the electron fluctuation frequency from $\nu < \nu_0$ to $\nu > \nu_0$, with ν_0 the NMR frequency of about 10^8 s^{-1} – these 24 lines become reduced to a mere doublet, corresponding to the averaged contributions of the A- and B-site signals, respectively; and that (ii) below T_V charge disproportionation is revealed to a comparable amount as reported from LSDA + U analyses [35–39]. In particular, the effect of motional narrowing, being resolved also in further NMR [42, 43] and Mössbauer investigations [42, 44, 45], disproves the presumption [5, 6] of itinerant electrons, fluctuating below T_V with frequencies of about 10^{16} s.

with them, as well as with our basic experimental MAE results on magnetite. This leads us to interpret in the following the observed MAE spectra on a minimum basis of elementary, experimentally well corroborated arguments:

(1) below T_V, the Fe ions reside on electromagnetically *different* B-sites – as directly ascertained by the mere *occurrence, itself,* of pronounced MAEs;
(2) below T_V, the 3d-t_{2g} band is split up into two sub-bands, being separated by a *minor gap* enclosing the Fermi level [38], which may be crossed by thermally excited electrons – in agreement with the thermally activated nature of the observed electronic processes, cf section 4.1, [2, 12, 35–39];
(3) only electrons situated near to the gap are contributing to the charge transport processes, as observed experimentally by means of EC and MAE experiments.

4.2.2. Timescale-conform elementary MAE analysis.

4.2.2a. A not too wide gap – of the order of 0.05 eV $< Q_G <$ 0.3 eV, [2, 12, 35–39] – formed on cooling down below T_V due to spontaneous band-splitting, thereby separating a full valency from a depopulated conduction band, offers the chance of becoming bridged by thermally activated electrons in the form of hopping (at elevated temperatures) or incoherent tunnelling (at lower temperatures).

As possible candidates, among the MAE spectra, for such hopping – versus incoherent tunnelling (figure 6) – at first, either of the two relaxation plateaus (4 K $< T <$ 35 K) and (50 K $< T <$ 125 K) may be feasible, cf figure 1. Considering, however, their respective activation enthalpies (table 1) and extremely different perturbation-sensibility (sections 3.2.1, 3.2.2) – with electron tunnelling assumed to be the more defect-sensitive process – the upper plateau is identified with thermally activated hopping. As found in preceding conductivity

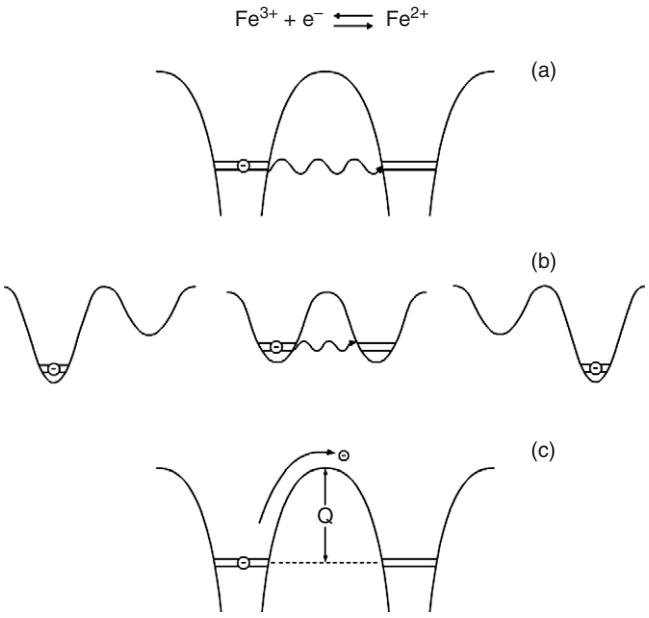

Figure 6. Illustration of various mechanisms of electron transport in magnetite: (a) coherent tunnelling, (b) incoherent tunnelling, (c) thermally activated hopping.

studies on magnetite, cf section 4.1 [33], and correspondingly Ti-doped magnetite [23, 46], this process follows a $T^{-1/4}$ activation, as being regarded characteristic for *variable-range electron hopping* [34].

Accordingly, the effects of dilute Ti-doping on the upper relaxation plateau (cf section 3.2.2) are explained as follows: (i) the *impurity-increased* relaxation strength as resulting from enhanced hopping, due to defect-induced, minor, gap width modulation; (ii) the *unbalancing of the plateau amplitudes* upon continued doping, as preferential closer-range hopping between perturbation centres with correspondingly reduced activation enthalpies; (iii) the *impurity-dependent shift* of the Verwey transition to lower temperatures, as indicating defect-induced destabilization of crystal structure upon whose transformation, at T_V, the electron exchange rates (equation (1)) are incremented – by shrinkage or even complete disappearance of the gap – above the detection limit of the MAE.

4.2.2b. Interestingly, *incoherent electron tunnelling*, to which the lower plateau (4 K $<$ T $<$ 25 K) is assigned [15–20], is found, in electric conductivity, to follow the same specific $T^{-1/4}$ law (figure 5), as the upper plateau (a) [33], cf section 4.1. Another, interesting feature of the magnetite spectrum consists in the pronounced 30 K Debye-type double peak (figure 1), cf section 3.2.3, which shows no influence on the thermally activated conductivity (section 4.1) and therefore has been attributed to *intra-ionic* thermal inter-level excitations (figure 7), [15, 16].

In terms of the 'one-ion' energy level systems (figure 7), low-temperature incoherent tunnelling (figure 6(b)) is associated with an *inter-ionic* exchange of the sixth electron between the lowest lying doublet states of adjoining Fe^{2+}, Fe^{3+} ions (figure 7(a)). Departing from a certain amount of phonon interaction, coinciding evidently with the breakdown of low-temperature tunnelling, this sixth electron is *intra-ionically* excited from the groundstate, across the gap between the trigonally split t_{2g} ($d\epsilon$) states, thereby inducing a variation of local anisotropy by either annihilation (figure 7(a), H_t $<$ 0) or creation (figure 7(b), H_t $>$ 0) of residual orbital momentum, giving rise to the pronounced 30 K peak [15, 16].[9]

Thus, the pronounced effects of dilute Ti-doping on the electronic processes contributing to the low-temperature MAE spectrum (4 K $<$ T $<$ 35 K) may be discussed in the following way:

(i) narrowing of the plateau, together with decreasing relaxation strengths, as being caused by a perturbation of inter-atomic e^--tunnelling (equation (1)) due to the replacement of one Fe^{3+} by one Ti^{4+} ion within the B-site quadruples (cf [2]), initially occupied by Fe^{2+} and Fe^{3+} ions as indicated by the square brackets:

$$[2Fe^{2+} + 2Fe^{3+}] + Ti^{4+} \longrightarrow [3Fe^{2+} + Ti^{4+}] + Fe^{3+}. \tag{9}$$

(ii) concomitant shift of the intra-ionically excited Debye peak – from initially 30 K to lower temperatures – as resulting from an impurity-induced perturbation of the corresponding ionic level-systems (figures 7(a), (b)).[10]

[9] By assuming the two signs of H_t to occur equally likely within the action range of a domain wall – which appears feasible when regarding the rotation of the spontaneous magnetization inside the wall, in addition to the effect of alternately changing H_t-directions (by about 110°) between adjoining, B-sited Fe ions – the double nature (cf table 1) of the 30 K maximum (section 3.2.3) finds its natural explanation. Thereby, the larger and smaller of the two enthalpies may be associated, respectively, with excitations from the lower-lying doublet groundstate (figure 7(a)) and from the singlet state (figure 7(b)), cf table 1, [15, 16].

[10] For instance, Ti^{4+} substitution according to (i) is expected to concomitantly induce attenuation of the trigonal and strengthening of the cubic crystal-field component, cf [1]. In proportion to the consequently diminished trigonal level-splitting (figure 7), thermal process activation is shifted to lower temperatures – ending finally, in combination with effects (i), into the observed, heavily damaged MAE residuals (figures 2, 3).

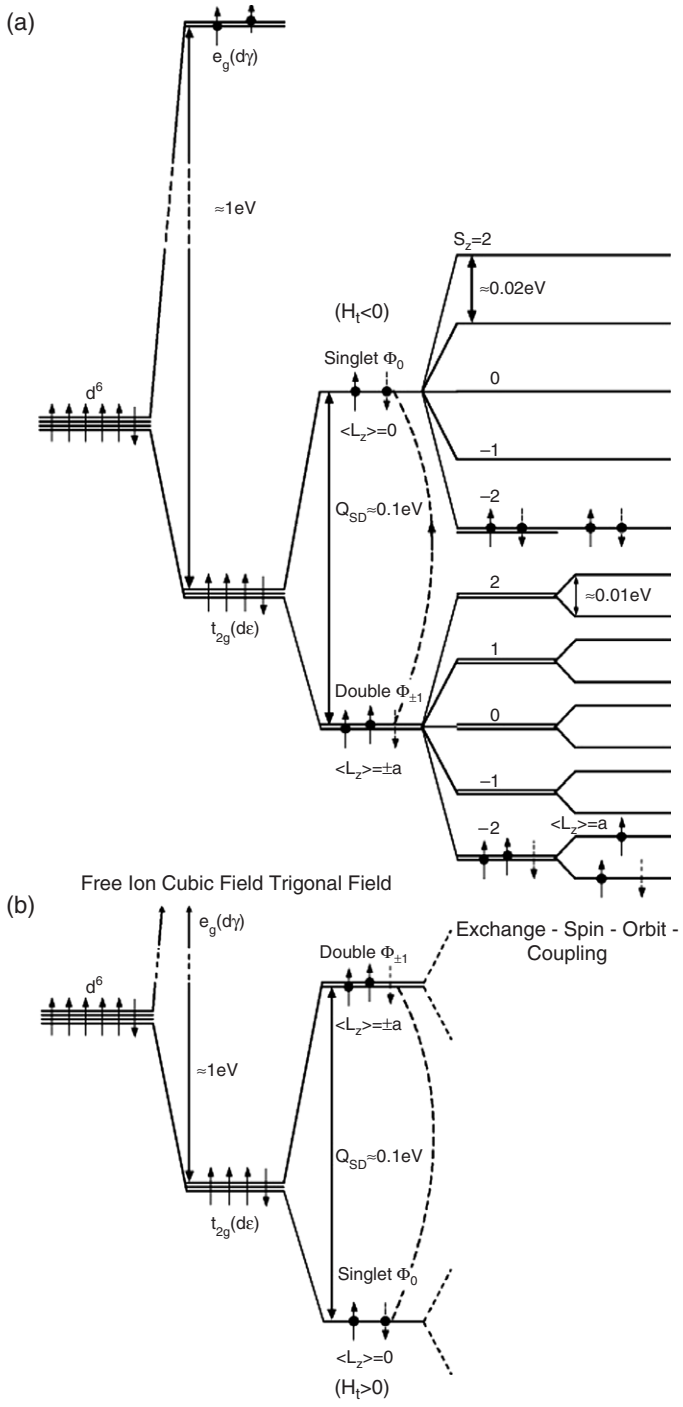

Figure 7. One-ion model, illustrating the energetic level splitting of octahedrally sited Fe^{2+} ions in the magnetite spinel lattice, being exposed to crystal-field (cubic, trigonal) and magnetic (exchange and spin-orbital coupling) interactions. Of importance for the low-temperature, intra-ionic excitation (30 K peak) is the type of realized trigonal splitting, i.e., (a) doublet ($H_t < 0$) or (b) triplet groundstate (H_t) > 0, cf section 4.2.2b.

4.2.2c. In the high-temperature range ($T > T_V$), due to drastically increased mobility, electronic transport processes become inaccessible to the MAE, so that in perfectly oxygen-stoichiometric crystals (figures 1–3) no further relaxations are observable (cf section 1, [1, 2, 15–22]) and, consequently, no *direct information* is available any more on high-temperature conductivity mechanisms.

Interestingly, however, *indirect information* on *high-temperature conductivity* is still deducible from high-purity, B-site vacancy-doped magnetite, $Fe_{3-x-\Delta}O_4$, [17–22]. Such crystals are characterized by the occurrence of a pronounced MAE maximum near 300 K, resulting from vacancy-mediated ionic (Fe^{2+}) hopping, which has been identified as being composed of two single Debye processes with slightly differing activation enthalpies. The corresponding enthalpy difference, of about 0.06 eV [17–22] (table 1), is associated with two modified activation modes corresponding, besides (i) hopping of as-ready Fe^{2+} ions (with $Q \simeq 0.85$ eV), to (ii) additional hopping of Fe^{3+} ions which, before transmuting into MAE-relevant anisotropic Fe^{2+} ions, have to attract a thermally activated electron, thus yielding an increased enthalpy of about $Q \simeq 0.85 + 0.06 \simeq 0.91$ eV (table 1).

Accordingly, we concluded the electron mobility above the Verwey transition ($T_V < T < 350$ K) to be thermally activated[11] with this enthalpy difference of about 0.06 eV, the value of which compares well with the results determined from various other investigations [3, 23, 33, 47–50].

4.3. The actual state of magnetite research

4.3.1. Experimental basis for model designing. As described in the foregoing there is presently no well-defined model designable out of the vast amount of experimental material collected over about 60 years. Instead there exists a diffuse agglomeration of information obtained by means of a series of more or less sensitive techniques on a variety of more or less perfect magnetite crystals, discussed in terms of more or less appropriate hypothetical conceptions.

Against this amount of incertitudes, MAE spectroscopy – as shown in the preceding sections – has to be considered as the most sensitive instrument presently available for the determination of magnetite quality and the analysis of defect-induced deficiencies [2]. As outlined in the foregoing (cf section 4.2.1), the fundamental MAE results to be accounted for in any magnetite model, may be shortly formulated as follows.

(1) Octahedrally sited Fe ions in Fe_3O_4 are electronically inequivalent – thus providing the basis for the various types of MAEs observed.
(2) Low-temperature MAE processes in Fe_3O_4 result from thermal activation of electrons across a gap, separating – on cooling below T_V – a full valency from a depopulated conduction band.

[11] This thermal activation of the conductivity, in the interval $T_V < T < 350$ K, is clearly evident from figure 5, cf [33, 49]. Only by disregarding its *positive* temperature coefficient (figure 5) is the conductivity in magnetite often inadequately denoted as being of metal type – after having undergone an 'insulator–metal' transition at T_V. Strictly speaking, however, the Verwey transition represents a 'worse-to-better semiconductor' transition, accompanied by a spontaneous conductivity change at T_V (of about a factor of 100) and a badly comprehended, non-exponential thermal activation in the ensuing temperature range [2, 33, 49]). The notation 'semiconductor/semimetal' transition – by regarding the anomalous, high-temperature activation as a feasible result of two counteracting contributions [50] of, i.e., (i) 'normal' (exponential) thermal activation and (ii) temperature-dependent, metallic band-like electron–phonon scattering – may be tolerable, under the sole condition, however, of always being aware that thermal activation is the prevailing process [33, 49, 50].

4.3.2. Magnetite models presently under discussion. As outlined in section 1, the classical electronic transport processes, giving rise to electric conductivity and associated MAEs, can be most conveniently explained, to many details, in terms of the traditional Verwey–Mott conceptions [3, 4] which, however, suffer from the lasting handicap that their basic assumptions of (i) low-temperature long-range ordering[12] of (ii) well-segregated Fe^{2+} and Fe^{3+} ions could not be verified experimentally so far. Against this background – still enriched by their apparently, order-disproving XRS experiments – Garcia *et al* [5, 6] proclaimed the Verwey–Mott model to be regarded, from now on, as completely outdated and falsified. Our analysis shows, however, that this declaration appears premature under the following aspects:

(1) this deduction is mainly based on resonant x-ray and other – not always incontestable – diffraction experiments, without any consideration of the technologically most important conduction mechanisms. Even more unsatisfactory, no attempt is made to develop an alternative interpretation frame for these, innovation-decisive, effects;

(2) this declaration is in contradiction with modern electron-theoretical calculations, based on a variety of experimental data (cf section 4.2.1) [35, 38, 39] whose interpretation, interestingly, being in qualitative agreement with both our MAE results and the basic Verwey–Mott conceptions, arrive at the following conclusions: (i) the occurrence of different, though non-integral charge disproportionations of B-sited Fe ions, undergoing complicated long-range ordering below T_V; (ii) the appearance of an [100]-oriented charge density wave in connection with this specific low-temperature ordering which – via collective electronic screening effects – is supposed to also induce the observed charge disproportionations; (iii) the violation of the Anderson condition [40] which, within this interpretation frame, is a consequence of considering – besides conventional Coulomb interactions – additionally, the transition-induced contribution of lattice distortions.

(3) Following accurately Mott's considerations in deriving his low-temperature conductivity model, the enormous timescale difference as determined from either XRS or MAE may be explained as follows: whereas Garcia *et al* postulate their deduced electron fluctuation time, of about 10^{-16} s, to be representative for *all* octahedral sites in the spinel – and on account of this ultra-short value exclude the existence of electronically different Fe ions and their possible ordering in the low-temperature phase – according to Mott, only the (feasible) minority-group of electrons, being effectively engaged in charge transport, is able to participate in charge ordering. Thus, in terms of the above sketched, gap-separated, two-band system – with the lower band assumed to be completely filled-up by Fe^{2+} ions and the higher one, initially, weakly populated by Fe^{3+} ions – only the higher band, after thermal activation, disposes on the necessary minority group of both Fe^{2+}*and* Fe^{3+} ions being, possibly, able to participate in ionic ordering[13]. Thus, Garcia *et al*'s results may be understandable by assuming that their experimental conduct is unable to resolve the – relatively weak – contributions of the higher-band minority-group of electrons so that, consequently but erroneously, they take the effect of the low-band majority group alone as representative for the complete system.

[12] Here it appears noteworthy to mention that Wiesendanger *et al* [12], by means of scanning tunnelling microscopy, were able to resolve ionic short-range ordering, though under rather puzzling experimental conditions, such as, for example: (i) room-temperature, (ii) surface investigations of a (iii) *natural* single crystal, characterized by (iv) a Verwey-transition of only 98 K (!), cf section 1. In order to prove the relevance of these results, repetition of respective experiments under definite conditions – i.e., perfectly stoichiometric single-crystalline magnetite at temperatures below T_V – appears indispensable.

[13] This view, in terms of Mott's conceptions [4, 34], is confirmed by recent, experiment-based LSDA + U electron-theoretical calculations [38, 39] and, moreover, has been the fundament of a most efficient, two-level based theoretical analysis of the Verwey transition [51].

5. Summary

(1) The effects of dilute Ti-doping on the intrinsic MAE spectra of stoichiometric magnetite are discussed in terms of a revised low-temperature ($4\ \mathrm{K} < T < T_V \simeq 125\ \mathrm{K}$) model, based on the indispensable preconditions for the occurrence of MAEs, i.e.: (i) the existence of electronically, and hence magnetically, inequivalent sites in the octahedral (B-type) sublattice of magnetite; (ii) thermal activation of electron transport between the differently valent, B-site residing Fe ions, with relaxation times ranging from 1 s up to thousands of seconds.

(2) The two plateau-type MAE relaxation zones occurring in dilute Ti-doped Fe_3O_4 within the temperature ranges of $4\ \mathrm{K} < T < 35\ \mathrm{K}$ and $50\ \mathrm{K} < T < T_V$ are interpreted, respectively, with incoherent inter-ionic tunnelling, culminating in thermal intra-ionic excitation, and thermally activated electron hopping. The analysis of both plateaus yields deeper insights into electronic d-band splitting and low-temperature conductivity mechanisms.

(3) Our magnetite model, besides offering consistent interpretation of the low-temperature MAE spectra and electronic conductivity, is of even higher-ranking importance with respect to a final solution of the still-open magnetite dilemma. Thus, the rather *apodictically* propagated breakdown of the Verwey–Mott conceptions – as deduced from recent x-ray resonant scattering (XRS) yielding, independent of temperature ($T \lesssim T_V$), extremely short electron fluctuation times of about 10^{-16} s has to be relativized when confronted with our multiply corroborated magnetite model [2].

(4) The large discrepancy (of about a factor of 10^{20}) between the low-temperature electron relaxation times, determined by either XRS or MAE, is attributed to two different categories of electrons: (i) quickly fluctuating, filled-band ground-state electrons (XRS) and (ii) thermally activated electrons (MAE), crossing the Fermi level – via a transition-induced gap, separating a lower, Fe^{2+}-occupied band from a higher, faintly Fe^{3+}-populated state. After electronic gap-crossing, the upper band contains Fe ions of mixed valency, thus enabling the initiation of various conductivity mechanisms evoking related MAEs.

(5) Our present analysis, yielding thermal activation for all electronic low-temperature relaxation processes, is in basic agreement with recent electron-theoretical LSDA + U calculations, confirming the existence of two types of well-distinguished – though charge-disproportionated – Fe ions residing on the octahedral sites. The occurrence of charge disproportionation, in combination with a [100]-oriented charge density wave – in LSDA + U results – may be regarded as a consequence of collective screening effects connected with the deduced complex structure of ionic long-range ordering.

Acknowledgments

The authors remember gratefully many helpful discussions with Professor Dr M Fähnle and Dr E Goering. Their further thanks are addressed to Mr R Henes for his assistance during sample preparation and to Mrs I Schofron and Mr F W Gergen for their support in elaborating e-mail compatible text and figure presentations.

References

[1] Walz F, Brabers J H V J, Brabers V A M and Kronmüller H 2003 *J. Phys.: Condens. Matter* **15** 7029
[2] Walz F 2002 *J. Phys.: Condens. Matter* **14** R285
[3] Verwey E J W and Haayman P W 1941 *Physica* **8** 979
Verwey E J, Haayman P W and Romeijn F C 1947 *J. Chem. Phys.* **15** 181
[4] Mott N F 1979 *Festkörperprobleme* **19** 331
Mott N F 1980 The Verwey transition *Phil. Mag.* **42** (special issue) 327

[5] Garcia J, Subias G, Proietti M G, Blasco J, Renevier H, Hodeau J L and Joly Y 2001 *Phys. Rev.* B **63** 054110
[6] Garcia J and Subias G 2004 *J. Phys.: Condens. Matter* **16** R145
[7] Margulies D T, Parker F T, Spada F E, Goldman R S, Li J, Sinclair R and Berkowitz A E 1996 *Phys. Rev.* B **53** 9175
[8] Van der Zaag P J, Fontijn W F J, Gaspard P, Wolf R M, Brabers V A M, Van de Veerdonk R J M and Van der Heijden 1996 *J. Appl. Phys.* **79** 5936
[9] Ziese M and Blythe H J 2000 *J. Phys.: Condens. Matter* **12** 13
[10] Morall P, Schedin F, Case G S, Thomas M F, Dudzik E, Van der Laan G and Thornton G 2003 *Phys. Rev.* B **67** 214408
[11] Watts S M, Nakajima K, Van Dijken S and Coey J M D 2004 *J. Appl. Phys.* **95** 7465
[12] Wiesendanger R, Shvets I V and Coey J M D 1994 *J. Vac. Sci. Technol.* **12** 2118
[13] Park S K, Ishikawa T and Tokura Y 1998 *Phys. Rev.* B **58** 3717
[14] Antonov V N, Harmon B N and Yaresko A N 2003 *Phys. Rev.* B **67** 024417
[15] Walz F, Weidner M and Kronmüller H 1980 *Phys. Status Solidi* a **59** 171
[16] Kronmüller H and Walz F 1980 *Phil. Mag.* B **42** 433
[17] Walz F, Brabers V A M, Chikazumi S, Kronmüller H and Rigo M O 1982 *Phys. Status Solidi* b **110** 471
[18] Walz F and Kronmüller H 1990 *Phys. Status Solidi* b **160** 661
Walz F and Kronmüller H 1994 *Phys. Status Solidi* b **181** 485
[19] Walz F and Kronmüller H 1991 *Phil. Mag.* **64** 623
[20] Walz F, Brabers V A M and Kronmüller H 1997 *J. Physique Coll.* **7** C1 569
[21] Kronmüller H, Schützenauer R and Walz F 1974 *Phys. Status Solidi* a **24** 487
[22] Walz F, Rivas J, Brabers J H V J and Kronmüller H 1999 *Phys. Status Solidi* a **173** 467
[23] Kuipers A J M and Brabers V A M 1979 *Phys. Rev.* B **20** 594
[24] Smiltens J 1952 *J. Chem. Phys.* **20** 990
[25] Muan A and Osborn E F 1965 *Phase Equilibria Among Oxides in Steelmaking* (Oxford: Addison-Wesley)
[26] Kuipers A J M and Brabers V A M 1976 *Phys. Rev.* B **14** 1401
[27] Walz F 1971 *Phys. Status Solidi* a **8** 125
Walz F 1974 *Appl. Phys.* **3** 313
Walz F 1984 *Phys. Status Solidi* a **82** 179
Walz F 1995 *Phys. Status Solidi* a **147** 237
[28] Seeger A, Kronmüller H and Rieger H 1965 *Z. Angew. Phys.* **18** 377
[29] Kronmüller H 1968 *Nachwirkung in Ferromagnetika* (Berlin: Springer)
[30] Blythe H J, Kronmüller H, Seeger A and Walz F 2000 *Phys. Status Solidi* a **181** 233
[31] Walz F, Brabers J H V J and Brabers V A M 2002 *Z. Metallk.* **93** 1095
[32] Smit J and Wijn H P J 1959 *Ferrites* (New York: Wiley)
[33] Lenge N, Kronmüller H and Walz F 1984 *J. Phys. Soc. Japan* **53** 1406
[34] Mott N F 1974 *Metal–Insulator Transitions* 1st edn (London: Taylor and Francis)
[35] Wright J P, Attfield J P and Radaelli P G 2001 *Phys. Rev. Lett.* **87** 266401
Wright J P, Attfield J P and Radaelli P G 2002 *Phys. Rev.* B **66** 214422
[36] Antonov V N, Harmon B N, Antropov V P, Berlov A Y and Yaresko A N 2001 *Phys. Rev.* B **64** 134410
[37] Anisimov V I, Aryasetiawan F and Lichtenstein A I 1997 *J. Phys.: Condens. Matter* **9** 767
[38] Jeng H-T, Guo G Y and Huang D J 2004 *Phys. Rev. Lett.* **93** 156403
[39] Leonov I, Yaresko A N, Antonov V N, Korotin M A and Anisimov V I 2004 *Phys. Rev. Lett.* **93** 146404
[40] Anderson P W 1958 *Phys. Rev.* **109** 1492
[41] Novak P, Stepankova H, Englich J, Kohout J and Brabers V A M 2000 *Phys. Rev.* B **61** 1256
[42] Iida S, Mizushima K, Mada J, Umemura S, Nakao K and Yoshida J 1976 *AIP Conf. Proc.* vol 29, p 388
[43] Mizoguchi M 2001 *J. Phys. Soc. Japan* **70** 2333
[44] Hargrove R S and Kündig W 1970 *Solid State Commun.* **8** 203
[45] Berry F J, Skinner S and Thomas M F 1998 *J. Phys.: Condens. Matter* **10** 215
[46] Brabers V A M 1995 *Physica* B **205** 143
[47] Broese van Groenou A, Bongers P F and Stuits A L 1968/69 *Mater. Sci. Eng.* **3** 317
[48] Brabers V A M 1995 Progress in spinel ferrite research *Handbook of Magnetic Materials* ed K H Buschow (Amsterdam: Elsevier)
[49] Miles P A, Westphal W B and von Hippel A 1957 *Rev. Mod. Phys.* **29** 279
[50] Ihle D and Lorenz B 1986 *J. Phys. C: Solid State Phys.* **19** 5239
[51] Brabers J H V J, Walz F and Kronmüller H 1999 *Physica* B **266** 321
[52] Braginski A 1965 *Phys. Status Solidi* **11** 603
[53] Castro J, Rivas J, Blythe H J, Iniguez J and De Francisco C 1989 *Phys. Status Solidi* a **113** 541